Materials Science & Engineering C 107 (2020) 110209

Contents lists available at ScienceDirect

Materials Science & Engineering C

journal homepage: www.elsevier.com/locate/msec

Synthesis and utilization of Co_3O_4 doped carbon nanofiber for fabrication of hemoglobin-based electrochemical sensor

Hui Xie[a], Guiling Luo[a], Yanyan Niu[a], Wenju Weng[b], Yixing Zhao[a], Zhiqiang Ling[a], Chengxiang Ruan[c], Guangjiu Li[b], Wei Sun[a,*]

[a] Key Laboratory of Laser Technology and Optoelectronic Functional Materials of Hainan Province, College of Chemistry and Chemical Engineering, Hainan Normal University, Haikou, 571158, PR China
[b] Key Laboratory of Optic-electric Sensing and Analytical Chemistry for Life Science of Ministry of Education, College of Chemistry and Molecular Engineering, Qingdao University of Science and Technology, Qingdao, 266042, PR China
[c] Jiangxi Key Laboratory of Surface Engineering, Jiangxi Science and Technology Normal University, Nanchang, 330013, PR China

ARTICLE INFO

Keywords:
Hemoglobin
Cobalt oxide doped carbon nanofiber
Biosensing
Direct electrochemistry
Electrocatalysis

ABSTRACT

In this paper cobalt oxide (Co_3O_4) nanoparticles were mixed with polyacrylonitrile to prepare Co_3O_4 doped carbon nanofiber (CNF) composite by electrospinning and carbonization, which was further used to modify on carbon ionic liquid electrode (CILE). Hemoglobin (Hb) was immobilized on Co_3O_4–CNF/CILE surface with Nafion acted as the protective film to fabricate an electrochemical biosensor (Nafion/Hb/Co_3O_4–CNF/CILE). Electrochemical behavior of Hb on the electrode was investigated with a pair of quasi-reversible redox peak appeared on cyclic voltammogram and electrochemical parameters were calculated. Moreover, this biosensor had good analytical capabilities for electrocatalytic reduction of different substrates including trichloroacetic acid, potassium bromate and sodium nitrite with wider detection range from 40.0 to 260.0 mmol L^{-1}, 0.1 to 48.0 mmol L^{-1} and 1.0 to 12.0 mmol L^{-1} by cyclic voltammetry, respectively. The proposed method showed excellent anti-interferences ability with good selectivity and was successful used for quantitative detection of real samples, which displayed the potential applications to develop into a new analytical device.

1. Introduction

Electrochemical biosensor is based on the changes of electric signal when the biochemical receptor on the working electrode has selective response to the analyte. Redox enzyme/protein is usually used as a chemical selective layer over a highly conductive support material/matrix, which can transmit biochemical signals to electrical signals after recognizing the appropriate detection target [1,2]. Hemoglobin (Hb) is one of the most commonly used redox protein for electrochemical investigation [3,4]. However, it is difficult to obtain direct electron transfer of Hb due to three-dimensional macrostructure of protein that results in inaccessibility of the electroactive center to electrode or the strong adsorption on electrode surface [5]. Also, the unusual alignment of biomolecules on the electrode surface can be one of the reasons for inhibiting electron transfer between protein and the electrode [6]. Therefore, a facile electron transfer path between the biocatalytic reaction and electrode is necessary to establish, which can improve the functional properties of biosensor as well as to maintain high electro-activity of protein on the electrode surface. Baghayeri et al. investigated direct electrochemistry of Hb on carbon material/metal oxide based nanocomposite for hydrogen peroxide analysis [7–10]. Chen's group studied direct electron transfer of Hb on various nanomaterials modified electrodes [11–16]. Radhakrishnan et al. constructed enzymatic biosensor for the electrocatalysis investigation of hydrogen peroxide and nitrite [17,18].

Recent advances of nanoscience promote the development of nanobiosensors with high sensitivity, more precise, excellent selectivity, fast response and easy operation [19–21]. Modification of the transducer surface with nanomaterials brings novel and unique properties, which show the ability to provide an effective and stable platform for biological sensing [22–24]. Therefore, integration of nanomaterials into the sensing layer is usually accompanied by fast mass transfer rate with acceleration of the transduction process [25–27]. Among various nanomaterials used, nanofiber (NF) produced by electrospinning has attracted much attentions with its applications in physical or chemical sensors [22]. Carbon nanofiber (CNF) shows excellent physicochemical properties including large surface area, high aspect ratio, mechanical stability, broad chemical modification capacity, biocompatibility, good

* Corresponding author.
E-mail address: swyy26@hotmail.com (W. Sun).

https://doi.org/10.1016/j.msec.2019.110209
Received 21 March 2019; Received in revised form 2 September 2019; Accepted 15 September 2019
Available online 30 October 2019
0928-4931/

adhesion and superior dispersion, which has been exploited in various applications [28]. Also, CNF cooperated with conductive and electroactive support materials can take advantage of synergistic effects to obtain novel composites [20]. For example, Zhang et al. prepared a nitrogen-doped carbon nanoparticles-embedded CNFs material by thermal treatment of electrospinning polypyrrole nanoparticles/polyacrylonitrile (PAN) composite nanofibers [29]. Guo et al. prepared flexible TiCNFs by electrospinning for the fabrication of glucose sensor [30]. Mondal et al. incorporated Ag nanoparticles with CNFs to improve the electrochemical detection of triglyceride [31]. Zhu et al. synthesized a 3D CdS@CF networks by solvothermal process, which was used to construct an immunoassay sensor for photoelectrochemical bioanalysis [32].

Due to the excellent reversible redox ability, large specific area, semi-conductivity, great catalytic performance, long service life, good corrosion resistance and chemical stability [33,34], cobalt oxide nanoparticles (Co_3O_4 NPs) have been applied in various fields including batteries, sensors, catalysts, electronic devices and supercapacitors [35–38]. However, the semi-conductivity of Co_3O_4 NPs limits the applications in electrochemistry, which can be overcame by introducing highly conductive materials. In this paper, electrospinning Co_3O_4-PAN fiber was prepared and further carbonized to get Co_3O_4–CNF composite, which was acted as the sensitization material for the construction of electrochemical biosensor. Due to the best electrochemical performances of CNF, Co_3O_4 NPs were doped into CNF to obtain the nanocomposite by using electrospinning with the following carbonization, which combined the advantages of individual materials used. During electrospinning Co_3O_4 NPs can be uniformly dispersed in the PAN solution, which result in the well dispersion of Co_3O_4 NPs in the following carbonization with the formation of CNF. Co_3O_4 NPs exhibit its good biocompatibility with oxygenal groups present for the interaction of proteins. The structure of CNF is remained with higher conductivity and the long distance electron transfer is benefit for the electrochemistry of redox protein. Therefore the Co_3O_4–CNF nanocomposite combines the high electrochemical conductivity and good biocompatibility with novel synergistic effects for the immobilization of redox protein. The detailed process was illustrated in Scheme 1, and the fabricated sensor exhibited excellent stability, reproducibility and sensitivity for the electrochemical detection of trichloroacetic acid (TCA), potassium bromate ($KBrO_3$) and sodium nitrite ($NaNO_2$).

2. Experimental

2.1. Materials and reagents

Graphite powder (Shanghai Colloid Chem. Co. Ltd., China), N-hexylpyridinium hexafluorophosphate ($HPPF_6$, Lanzhou Yulu Fine Chem. Co. Ltd., China), Hb (Sigma-Aldrich. Co. Ltd., USA), Nafion (Du Pont. Co. Ltd., USA), PAN (J&k Scientific. Co. Ltd., China) and Co_3O_4 NPs (average diameter of 50 nm, Nanjing XFNANO Materials Tech. Co. Ltd., China) were used as received. All of the reagents were of analytical grade and phosphate buffer solution (0.1 mol L^{-1} PBS) were prepared as the supporting electrolytes, which required deoxygenation before electrochemical tests.

2.2. Apparatus

CHI 604E electrochemical workstation (Shanghai CH Instrument, China) was connected with a three-electrode model, which was made up of Nafion/Hb/Co_3O_4–CNF/CILE (the working electrode), saturated calomel electrode (SCE, the reference electrode) and platinum electrode (the counter electrode). JSM-7100F scanning electron microscope (JEOL, Japan), Nicolet 6700 FT-IR spectrophotometer (Thermo Fisher Scientific Inc., USA), TU-1901 double-beam UV–visible spectrophotometer (Beijing General Instrument Ltd. Co., China), D/Max-2500V X-ray diffractometer (Rigaku, Japan) with Cu-Kα radiation (λ = 1.54178 Å), raman spectrum (Horiba, France) with a LabRAM HR system using 532 nm lasers, X-ray photoelectron spectroscopy (AXIS HIS 165 spectrometer, Kratos Analytical, UK), STA-499F3 Jupiter synchronous thermal analyzer (NETZSCH, Germany), BTF-1200C vacuum tube furnace (Anhui Kemi Machinery Technology Co. Ltd., China) were used in the experiments.

2.3. Synthesis of Co_3O_4–CNF composite

Electrospinning equipment was composed of a DC high voltage power with adjustable voltage, a syringe with a pump, a spinneret with a metallic needle and a rotating collection device with a speed regulator, which was self-constructed in our lab. The Co_3O_4 blended PAN fiber was prepared based on references [31,39,40]. Briefly, 2.80 g PAN was dissolved in 35 mL N,N-dimethylformamide with 1 h ultrasonic oscillation to obtain a 8.00% polymer solution, which was further mixed with 0.70 g Co_3O_4 nanoparticles to get an electrospun solution. Spinning was operated under the electrostatic filed with the voltage as 17.27 kV. The speed of the collecting device was 1450 rpm, and the gap between metal nozzle and collector was 18 cm. The flow rate of the syringe pump was 25.00 μL min^{-1} and the movement distance between left and right of the spinneret was 30 mm. After 24 h, the precursor fiber (Co_3O_4-PAN) was collected on the tin foil.

The programmed temperature method was adopted and Co_3O_4-PAN was carbonized in a vacuum tube furnace where nitrogen was continuously introduced. Briefly, at the first step the temperature was raised to 300 °C at a rate of 5 °C min^{-1} and to 800 °C with the rate as 10 °C min^{-1} at the second step. Then the temperature was maintained at 800 °C for 2 h completely carbonization. Finally, Co_3O_4–CNF composite was obtained after annealing.

2.4. Construction of electrochemical biosensor

CILE was prepared according to the previous report [41] and used as the basic electrode (Φ = 4 mm), which was polished smooth before modification. The as-prepared Co_3O_4–CNF was ultrasonically dispersed in deionized water to get a solution with the final concentration of 1.2 mg mL^{-1}, which was applied on CILE surface with the volume of 6 μL. After drying in air, 8 μL 15 mg mL^{-1} Hb solution was covered on Co_3O_4–CNF/CILE surface and dried naturally. Finally, 6 μL 0.5% Nafion was spread on Hb/Co_3O_4–CNF/CILE, which acted as a protective film. After drying in air, the working electrode (Nafion/Hb/Co_3O_4–CNF/CILE) was constructed.

3. Results and discussion

3.1. Characterization of Co_3O_4–CNF composite

The precursor PAN fiber and its derived CNF were characterized by SEM with the images shown in Fig. 1A and B, respectively. It could be seen that the fiber remained its original size and smooth surface without swelling or condensation after carbonization. The SEM images of as-prepared Co_3O_4–CNF were shown in Fig. 1C–E, it could be found that some bright spots were observed on CNF surface, which were part of Co_3O_4 NPs embedded in CNF and the fiber average diameter was 400 nm. Fig. 1F displayed the morphology of Co_3O_4 NPs used in this experiment, which was commercial available with the average diameter of 50 nm. After it was dissolved in PAN polymer solution with fully ultrasonic and oscillation, a uniform solution could be obtained without the agglomeration. Therefore at the synthesized Co_3O_4–CNF nanocomposite, uniform distribution of Co_3O_4 NPs could be found within CNF and on the surface of CNF.

Raman spectra of CNF (curve a) and Co_3O_4–CNF (curve b) were presented in Fig. 1G with two bands appeared at 1319 cm^{-1} and 1589 cm^{-1}, which were corresponded to D and G bands of carbon, respectively. The D/G band intensity ratio (denoted by I_D/I_G) is

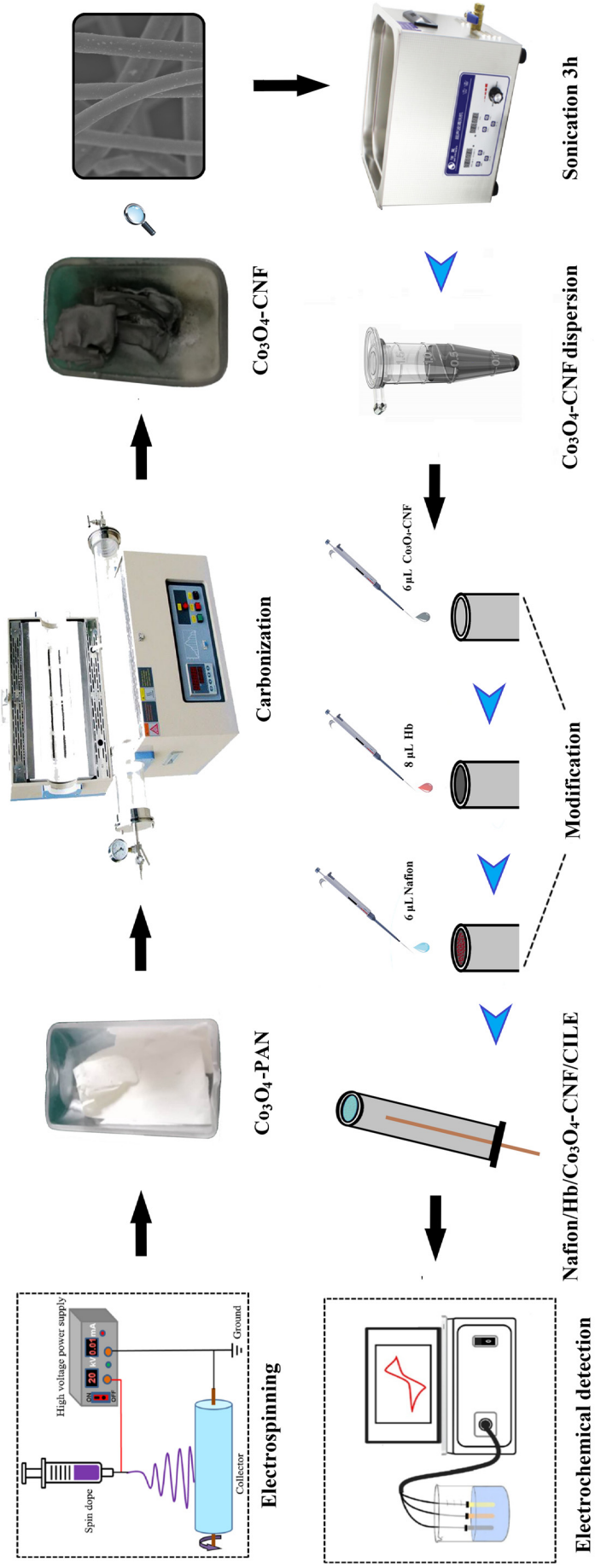

Scheme 1. Electrospinning and carbonization for the synthesis of Co_3O_4–CNF nanocomposite with fabrication process of Nafion/Hb/Co_3O_4–CNF/CILE.

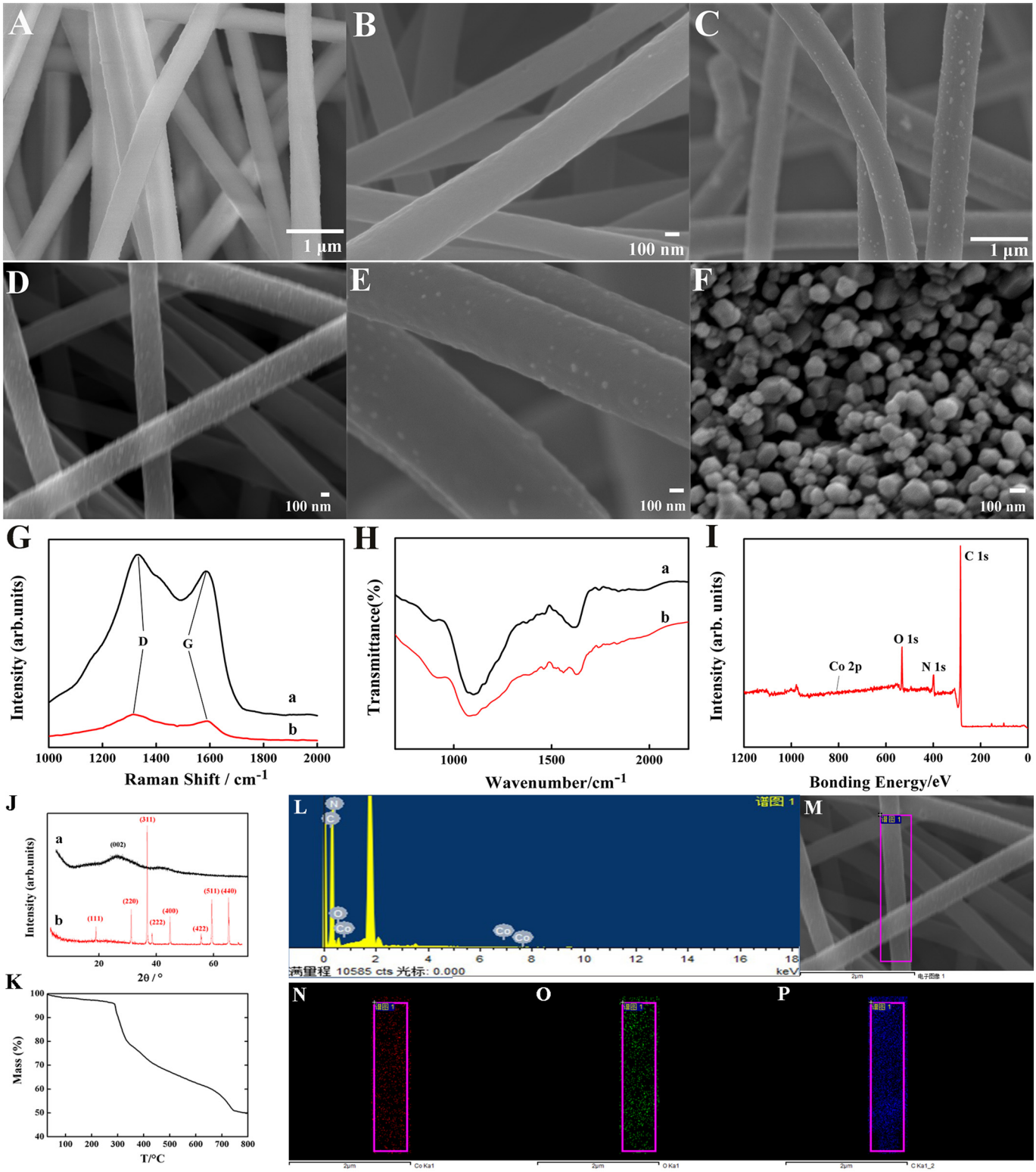

Fig. 1. SEM images of (A) PANF, (B) CNF, (C–E) Co_3O_4–CNF of different magnifications and (F) Co_3O_4; (G) Raman spectrum of (a) CNF and (b) Co_3O_4–CNF; (H) FT-IR of (a) CNF and (b) Co_3O_4–CNF; (I) XPS survey spectra of Co_3O_4–CNF; (J) XRD of (a) Co_3O_4–CNF and (b) Co_3O_4; (K) TG analysis of Co_3O_4-PANF; (L) EDS diagram of Co_3O_4–CNF; (M) The scanning area of element mapping and element mapping of (N) Co, (O) O and (P) C.

frequently used to evaluate the graphitic content in carbon samples [42]. The I_D/I_G ratio of CNF and Co_3O_4–CNF were calculated as 1.14 and 1.10, demonstrated that carbon graphitic layer grown and the spacing between two graphite layers decreased due to the presence of Co_3O_4 NPs that induced localized heating during the pyrolysis process, and then a highly graphitized carbon fiber was produced [31].

Fig. 1H presented FT-IR spectra of CNF (curve a) and Co_3O_4–CNF (curve b). The spectrum of CNF had strong peaks at 1105.44 $cm^{-1}$and 1629.19 cm^{-1}, which were assigned to the vibrations of C–N and C═C/C═N stretching [43]. After combined with Co_3O_4 NPs, Co_3O_4–CNF

Table 1
XPS components information of Co_3O_4–CNF.

Atom	Species	Peak BE	Atomic
C	1s	284.71 eV	83.28%
N	1s	398.13 eV	7.94%
O	1s	532.29 eV	8.62%
Co	2p	789.39 eV	0.16%

composite exhibited similar peaks to CNF and the decrease of peak intensities were resulted from the integrated Co_3O_4.

XPS can be used to distinguish the elements of composite. The XPS spectrum of Co_3O_4–CNF was shown in Fig. 1I, and the dominant peaks were distinctly indexed as O 1s, N 1s and C 1s regions with the component information shown in Table 1. While the content of Co element was extremely rare and difficult to be observed directly. In addition, the higher nitrogen content was due to the usage of PAN as the precursor, which contained abundant nitrogen source and its carbonization was also carried out under a nitrogen atmosphere.

XRD technique was used to analyze the components information of Co_3O_4 NPs and Co_3O_4–CNF with the data shown in Fig. 1J. All the X-ray diffraction peaks of Co_3O_4 NPs (curve b) could be indexed as (111), (220), (311), (222), (400), (422), (511) and (440) planes, which were assigned to cubic phase of Co_3O_4 that in good agreement with standard JCPDS card number 42–1467. As for Co_3O_4–CNF composite (curve a), an obvious peak at $2\theta = 26.0^\circ$ was attributed to the (002) reflection plane derived from carbon, indicating the formation of the graphite structure. However, no diffraction peak of Co_3O_4 crystal was emerged in this XRD pattern, which might be attributed to the relatively low content of Co_3O_4. No other impurity phases observed from the XRD analysis ensured the structural purity of the prepared Co_3O_4–CNF composite.

Fig. 1K displayed the thermogravimetric analysis of Co_3O_4-PANF with temperature raised to 800 °C in nitrogen atmosphere at a rate of 10 °C min^{-1}. As a result, 50% residual substance was obtained, which attributed to the thermal decomposition of PAN with partial mass loss. Because the prepared CNF–Co_3O_4 composite was the high temperature carbonized product of Co_3O_4-PANF in nitrogen at 800 °C, therefore the residual substance could be inferred as a mixture of carbon material and Co_3O_4. Moreover, Fig. 1L showed the EDS diagram of Co_3O_4–CNF composite with the elements of C, N, O and Co observed, which was in consistent with XPS characterization result. In order to clearly confirm the existence of Co_3O_4, the element mapping was carried out to check the distribution of Co element and the results indicated a uniform distribution of Co element (Fig. 1M to P).

3.2. Electrochemical characterization of Co_3O_4–CNF modified electrode

EIS can reflect the charge transfer resistance of the modified electrode by measuring the diameter of the semicircle and the obtained impedance data were fitted to Randles circuit by using the following elements including charge transfer resistance (Rct), electrolyte solution resistance (Rs), warburg element (W) and constant phase element (CPE). As shown in Fig. 2A, Co_3O_4–CNF/CILE (curve b) exhibited the smallest resistance (18.8 Ω) due to high conductivity of Co_3O_4–CNF. On Nafion/CILE the Rct value was increased to 339.8 Ω (curve c), suggested that non-conductive Nafion film blocked the electron transfer. The Rct of Nafion/Hb/CILE further increased to 413.6 Ω (curve d), indicated the presence of biomolecular Hb hindered the electron transport process. However, the Rct of Nafion/Hb/Co_3O_4–CNF/CILE was declined to 38.4 Ω (curve a), proved that the modification of highly conductive Co_3O_4–CNF could reduce the interface resistance as well as accelerate the electron transfer of $[Fe(CN)_6]^{3-/4-}$.

Electrochemical responses of different modified electrodes were also tested by CV with the curves shown in Fig. 2B. On CILE (curve c) a pair of quasi-reversible redox peaks displayed, and the modification of Co_3O_4–CNF on CILE (curve a) resulted in highest current responses of the redox peaks. However, the redox peak signals on Nafion/Hb/CILE (curve d) were reduced due to the presence of non-conductive Hb molecules and Nafion film that slowed the electron transfer rate. The current responses on Nafion/Hb/Co_3O_4–CNF/CILE (curve b) was significantly increased because Co_3O_4–CNF could provide a rapid path for electron transfer.

By using 1.0 mmol L^{-1} $[Fe(CN)_6]^{3-/4-}$ as the redox probe, cyclic voltammetric responses on Co_3O_4–CNF/CILE was tested under different scan rates (υ). Then the linear relationships between redox peak currents and $\upsilon^{1/2}$ were obtained as Ipc (μA) = 107.29 $\upsilon^{1/2}$ + 0.78 (n = 15, γ = 0.987) and Ipa (μA) = −90.38 $\upsilon^{1/2}$ - 2.46 (n = 15, γ = 0.985). Based on the Randles-Sevcik equation [44], the effective surface area (A) of Co_3O_4–CNF/CILE was calculated as 0.145 cm^2. Also the geometric surface area of CILE was calculated from the diameter of glassy electrode tube with the result as 0.126 cm^2. Therefore, the presence of Co_3O_4–CNF on the electrode could provide a larger surface area, which was beneficial to improve the adsorption capacity towards protein.

3.3. Electrochemical behavior of the Hb biosensor

Electrochemical behaviors of Hb on different electrodes were investigated and shown in Fig. 3A. As expected, neither oxidation nor reduction peak was observed on Nafion/Co_3O_4–CNF/CILE (c) and Nafion/CILE (d), indicating no electroactive substances existed with stable background currents. In contrast, a small pair of redox peaks appeared on Nafion/Hb/CILE (curve c), demonstrated the electron transfer of Hb was proceeded with slow rate. However, a pair of well-defined redox peaks with bigger current response appeared on Nafion/Hb/Co_3O_4–CNF/CILE (a), which proved that the presence of Co_3O_4–CNF was beneficial for fasten the electron transfer of Hb. The cathodic (Epc) and anodic (Epa) peak potentials of Nafion/Hb/Co_3O_4–CNF/CILE were observed at −0.325 V and −0.249 V, respectively. The formal potential ($E^{o\prime}$) was calculated as −0.287 V, which was the typical characteristic redox peaks of Fe(III)/Fe(II) in heme groups. The redox current ratio was close to 1.0 and the peak-to-peak potential (ΔEp) was 76 mV, revealed a quasi-reversible electron transfer process [45].

The effect of scan rate on the electrochemical responses of Nafion/Hb/Co_3O_4–CNF/CILE was investigated with the curves shown in Fig. 3B. Both the oxidation and reduction peak current increased with the increase of scan rate in the range of 20–800 mV s^{-1}. The linear regression equations were got as Ipc (μA) = 210.53 υ (V s^{-1}) + 11.59 (n = 17, γ = 0.996) and Ipa (μA) = −154.26 υ (V s^{-1}) - 8.53 (n = 17, γ = 0.994), indicated a surface-controlled process. By using equation Q = nAFγ* [46], the surface coverage of electroactive substance (γ*) was calculated as 4.73×10^{-9} mol cm^{-2}, higher than the theoretical monolayer surface concentration (1.89×10^{-11} mol cm^{-2}) [47]. The total amount of Hb on the modified electrode was 1.28×10^{-8} mol cm^{-2}, therefore 36.95% Hb was involved in the electrochemical reaction.

The separation of redox peak potentials also increased evenly with the increase of scan rate, and the linear relationship between redox peak potentials and lnυ was shown in Fig. 3C. Two regression equations were obtained as Epc (V) = −0.0568 lnυ (V s^{-1}) - 0.399 (n = 10, γ = 0.991) and Epa (V) = 0.0468 lnυ (V s^{-1}) - 0.151 (n = 10, γ = 0.994) at high scan rate range. According to the Laviron's equation [48], some relatively parameters such as the electron transfer number (n), the charge transfer coefficient (α) and the apparent heterogeneous electron transfer rate constant (k_s) were calculated as 0.99, 0.45 and 0.92 s^{-1}, respectively.

The influence of the buffer pH towards the electrochemical behavior of Hb in different pH PBS from 3.0 to 8.0 was shown in Fig. 3D. Obviously, the redox peak potentials shifted with pH changes, and it was easy to find the largest current response appeared at pH 5.0. Fig. 3E exhibited the linear relationship between $E^{o\prime}$ and pH with the regression

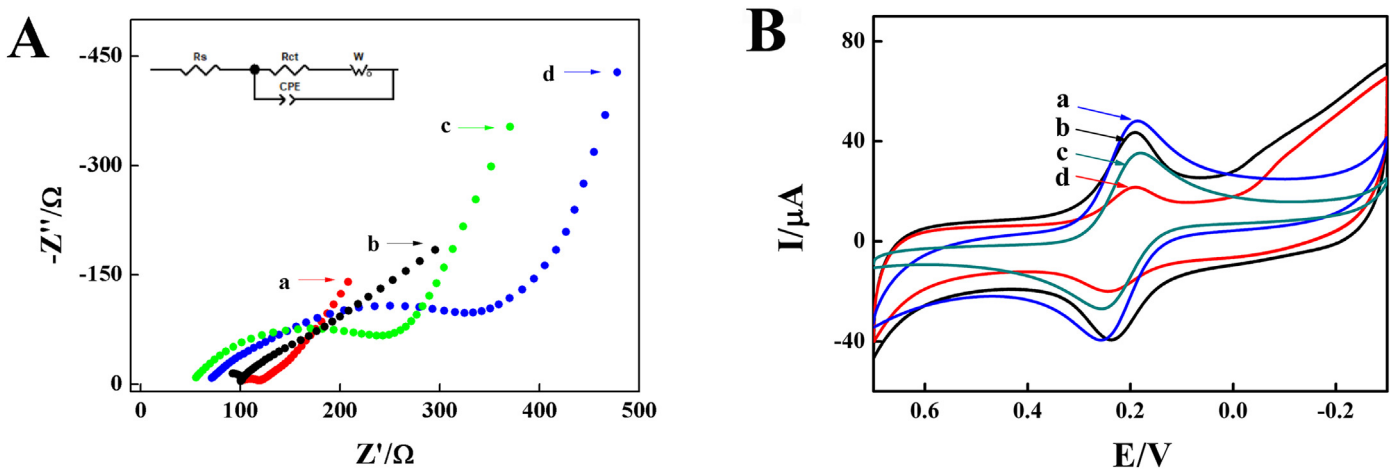

Fig. 2. (A) EIS patterns of Nafion/Hb/Co_3O_4–CNF/CILE (a), Co_3O_4–CNF/CILE (b), Nafion/CILE (c) and Nafion/Hb/CILE (d) with frequency from 10^4 to 0.1 Hz in a 10.0 mmol L^{-1} $[Fe(CN)_6]^{3-/4-}$ and 0.1 mol L^{-1} KCl mixture solution (Inset was the Randles equivalent circuit); (B) Cyclic voltammograms of Co_3O_4–CNF/CILE (a), Nafion/Hb/Co_3O_4–CNF/CILE (b), CILE (c) and Nafion/Hb/CILE (d) with the scan rate as 100 mV s^{-1} in a 1.0 mmol L^{-1} $K_3[Fe(CN)_6]$ and 0.5 mol L^{-1} KCl mixture solution.

equation as $E^{o\prime}$ (V) = −0.046 pH - 0.036 (n = 5, γ = 0.991). This slope value (−0.046 V pH^{-1}) was smaller than the theoretical value (−0.059 V pH^{-1}), inferred that the microenvironment slightly influenced Hb in the composite film, and also proved that Hb was involved in the redox reaction with same amount proton and electron transferred [49]. The influences of different kinds of buffers on the direct electrochemical behaviors of Hb modified electrode were also discussed with the results shown in Fig. 3F. As expected, in PBS (curve a), Britton-Robinson (curve b), citric acid-phosphate (curve c) and NaAc-HAc (curve d) a pair of redox peaks under pH 5.0 could be observed. However the biggest response appeared in PBS with better reversibility, which was selected as the supported electrolyte.

3.4. Electrocatalytic investigations

Electrocatalytic performance of Nafion/Hb/Co_3O_4–CNF/CILE towards TCA was investigated with cyclic voltammograms shown in Fig. 4A. The reduction peak current (Ipc) increased with TCA concentration while the oxidation peak current (Ipa) decreased continuously until disappeared. The first reduction peak appeared at -0.296 V and the second at −0.554 V, which were the typical electrocatalytic results. A good linear relationship between TCA concentration and the reduction peak current appeared with the detection range of TCA divided into two sections. As shown in Fig. 4B, the first one was from 4.0 to 40.0 mmol L^{-1} and the second from 40.0 to 260.0 mmol L^{-1} with the regression equations obtained as I_{ss} (μA) = 4.40 C (mmol L^{-1}) + 28.14 (n = 8, γ = 0.991) and I_{ss} (μA) = 1.70 C (mmol L^{-1}) + 146.40 (n = 9, γ = 0.991). The detection limit was 1.33 mmol L^{-1} (3σ).

Nafion/Hb/Co_3O_4–CNF/CILE was further used to explore the electrocatalytic reduction of $KBrO_3$, which was a stable anion with high solubility in water. As shown in Fig. 4C, electrochemical responses were recorded within the concentration range of $KBrO_3$ from 0.1 mmol L^{-1} to 48.0 mmol L^{-1}, which displayed that Ipc was increased with the continuous addition of $KBrO_3$ and Ipa was decreased until disappeared. The reduction peak appeared at −0.307 V and was constantly shifted right to - 0.703 V with the reaction proceeded. The linear regression equation between peak current and $KBrO_3$ concentration (Fig. 4 D) was obtained as I_{ss} (μA) = 17.58 C (mmol L^{-1}) + 47.93 (n = 13, γ = 0.991) and the detection limit was 0.033 mmol L^{-1} (3σ).

This Hb-based biosensor was also applied for the electrocatalytic detection of $NaNO_2$ and Fig. 4 E exhibited typical cyclic voltammograms of the reduction process. A new reduction peak appeared at −0.819 V and the peak current had a linear relationship with the concentration of $NaNO_2$ in the range of 1.0–12.0 mmol L^{-1}. As shown in Fig. 4 F, the linear regression equation was got as I_{ss} (μA) = 3.96 C (mmol L^{-1}) + 16.69 (n = 12, γ = 0.992) and the detection limit was 0.33 mmol L^{-1} (3σ). Moreover, a comparison of analytical parameters for $NaNO_2$ detection was listed in Table 2, which gave a relative wider linear range and lower detection limit.

Amperometric i-t method was also used for the quantification of TCA with Nafion/Hb/Co_3O_4–CNF/CILE and Fig. 5A showed the amperometric responses obtained at −0.55 V in pH 5.0 PBS. For every addition of TCA, there was a rapid increase in the catalytic current and then stabilized in 6 s. Linear response was achieved in the range from 1.0 mmol L^{-1} to 15.0 mmol L^{-1} with a sensitivity of 26.90 μA mM^{-1} cm^{-2} and 15.0 mmol L^{-1} to 120.0 mmol L^{-1} with a sensitivity of 586.90 μA mM^{-1} cm^{-2}. As shown in Fig. 5B, the regression equations were calculated as I_{ss} (μA) = 5.91 C (mmol L^{-1}) - 0.66 (n = 10, γ = 0.992) and I_{ss} (μA) = 2.88 C (mmol L^{-1}) + 54.98 (n = 12, γ = 0.992) with the detection limit as 0.33 mmol L^{-1} (3σ).

3.5. Analytical application

In order to check the practical applications of this Hb modified electrode, TCA content in the medical facial peel solution (purchased from Shanghai Ika Biotechnology Co. Ltd, China) and $NaNO_2$ content in the soak water of pickled vegetables (obtained from the local supermarket, Haikou, China) were determined by cyclic voltammetry and the recovery was estimated by the standard addition method. The samples of medical facial peel solution and soak water of pickled vegetables were diluted for 90 times and 25 times by using pH 5.0 PBS, respectively. As listed in Table 3, the contents of TCA and $NaNO_2$ were detected with the recovery range from 99.90% to 101.80% and 98.00%–101.00%, respectively. The relative standard deviation (RSD) were evaluated as 0.28%–1.95% and 0.31%–1.26%, which showed a reliable detection result.

3.6. Stability, reproducibility and selectivity

Cyclic voltammetric response of Nafion/Hb/Co_3O_4–CNF/CILE in pH 5.0 PBS was decreased for 8.98% after 150 cycles with the comparison of initial current. After stored at room temperature for 15 days, Nafion/Hb/Co_3O_4–CNF/CILE retained 97.64% of the original sensitivity, indicated good stability and easy preservation. Moreover, four times detection of 5.0 mmol L^{-1} TCA by the modified electrode gave the RSD as

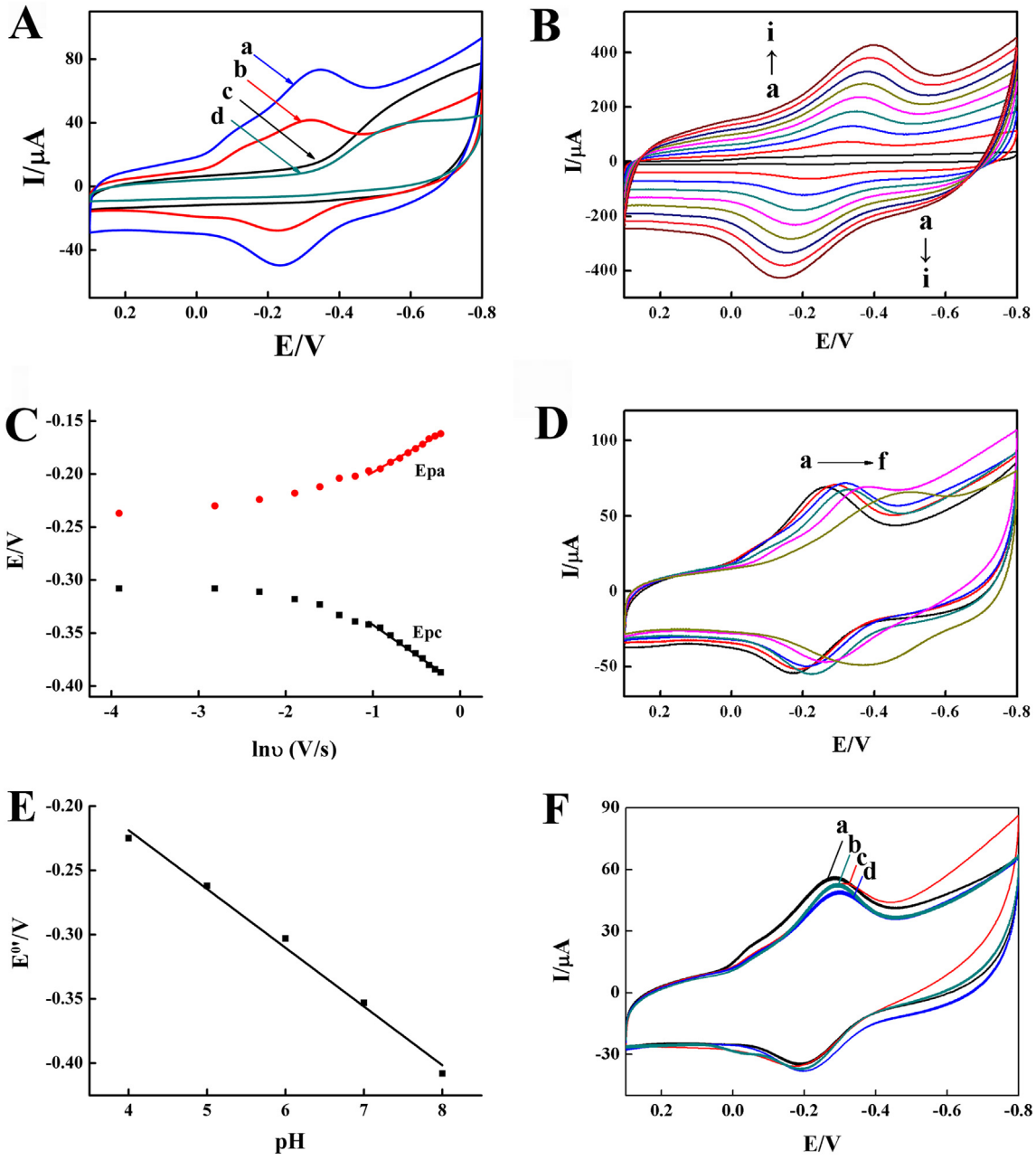

Fig. 3. (A) Cyclic voltammograms of (a) Nafion/Hb/Co_3O_4–CNF/CILE, (b) Nafion/Hb/CILE, (c) Nafion/Co_3O_4–CNF/CILE, (d) Nafion/CILE in pH 5.0 PBS at scan rate of 100 mV s^{-1}; (B) Influence of scan rate on redox reaction of Nafion/Hb/Co_3O_4–CNF/CILE in pH 5.0 PBS (from a to i as 20, 100, 200, 300, 400, 500, 600, 700, 800 mV s^{-1}); (C) The linear relationship of Epc and Epa vs lnυ; (D) Effect of pH on electrochemical response of Nafion/Hb/Co_3O_4–CNF/CILE at scan rate of 100 mV s^{-1} (from a to f 3.0, 4.0, 5.0, 6.0, 7.0, 8.0); (E) The linear relationship of $E^{o'}$ and pH; (F) Cyclic voltammograms of Nafion/Hb/Co_3O_4–CNF/CILE in pH 5.0 PBS (a), Britton-Robinson (b), citric acid-phosphate (c) and NaAc-HAc (d) at scan rate of 100 mV s^{-1}.

1.54%, reflected good reproducibility of this modified electrode.

Further, the selectivity of this biosensor towards the 4.0 mmol L^{-1} TCA was tested by amperometric method at −0.55 V in the presence of 5.0 mmol L^{-1} commonly interfering species including L-aspartic acid, L-valine, L-alanine, citric acid, Ba^{2+}, Ca^{2+}, K^+ and glucose in pH 5.0 PBS. However, no significant changes were observed after the addition of interfering species with the relative error less than 6.0%, and the results were shown in Table S1. Thus, the fabricated biosensor demonstrated good selectivity.

4. Conclusions

In this work, Co_3O_4 doped CNF was successfully synthesized, which appeared as fibrous network with large specific surface area, good conductivity and multiple active sites. By decoration of Co_3O_4–CNF on CILE interface, an interconnected structure with excellent electron transport capability was formed. After the immobilization of Hb and Nafion, an electrochemical biosensor was constructed with rapid electron transfer rate to achieve direct electrochemistry of Hb. This biosensor displayed great electrocatalytic properties towards TCA, $NaNO_2$ and $KBrO_3$, and the proposed method was further used to detect the real samples with excellent performance.

Acknowledgement

This project was supported by the Natural Science Foundation of

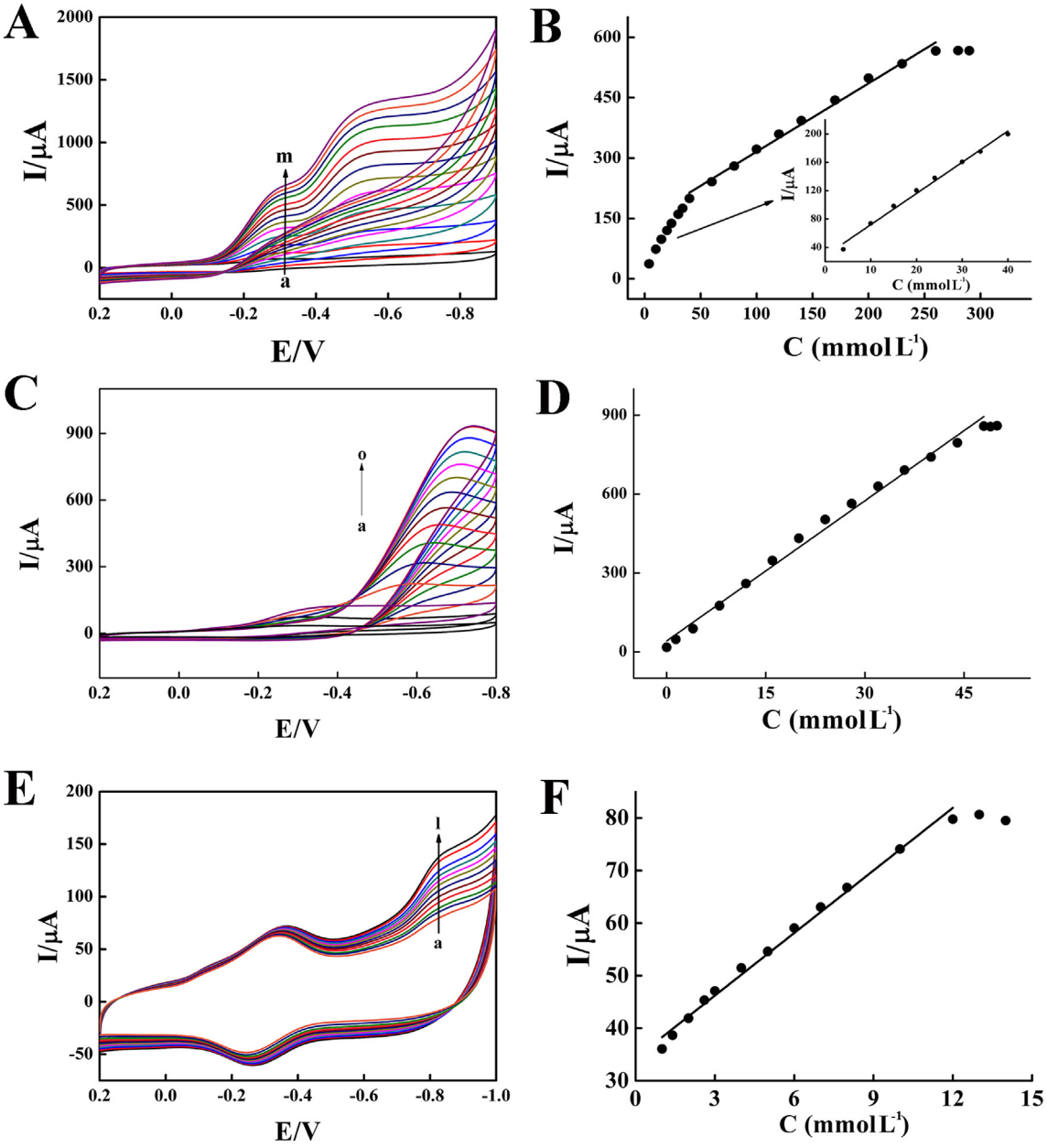

Fig. 4. Cyclic voltammograms of Nafion/Hb/Co_3O_4–CNF/CILE with (A) TCA (from a to m as 4, 10, 20, 40, 60, 80, 100, 120, 140, 170, 200, 230, 260 mmol L^{-1}), (C) $KBrO_3$ (from a to o as 0, 1.4, 4.0, 8.0, 12.0, 16.0, 20.0, 24.0, 28.0, 32.0, 36.0, 40.0, 44.0, 48.0, 49.0 mmol L^{-1}) and (E) $NaNO_2$ (from a to l as 1.0, 1.4, 2.0, 2.6, 3.0, 4.0, 5.0, 6.0, 7.0, 8.0, 10.0, 12.0 mmol L^{-1}) in pH 5.0 PBS at the scan rate of 100 mV s^{-1}; The linear relationship between peak currents with (B) TCA, (D) $KBrO_3$ and (F) $NaNO_2$ concentration.

Table 2
Comparison of analytical performance for $NaNO_2$ detection by various modified electrodes.

Modified electrodes	Analytical methods	pH	Applied potential (V)	Detection range (mmol L^{-1})	LOD (mmol L^{-1})	Ref.
Nafion/HRP/WS_2/CILE	Cyclic voltammetry	3.0	−0.61 V vs. SCE	1.5–4.0	0.20	[50]
CNF/Hemin/GCE	Hydrodynamic voltammetry	7.0	+0.3 V vs. Ag/AgCl	5.0–250.0	0.32	[51]
CTS-Hb-CNT-IL/CILE	Cyclic voltammetry	7.0	−0.806 vs. SCE	0.4–8.0	0.10	[52]
SA-Mb-IL-Fe_2O_3/CILE	Cyclic voltammetry	7.0	−0.91 V vs. SCE	4.0–100.0	1.30	[53]
Nafion/Mb-SWCNT/GCE	Square wave voltammetry	7.0	−0.7 V vs. Ag/AgCl	0.5–5.0	0.95	[54]
Hb-meso-Al_2O_3-PVA/GCE	Amperometry	6.5	−0.8 V vs. SCE	0.2–10.0	0.03	[55]
Nafion/Hb/Co_3O_4–CNF/CILE	Cyclic voltammetry	5.0	−0.819 V vs. SCE	1.0–12.0	0.33	This work

Hainan Province of China (2017CXTD007), the National Natural Science Foundation of China (21665007), the Key Science and Technology Program of Haikou City (2017042), and the Postgraduate Innovation Research Project of Hainan Province (Hys2018-211).

Appendix A. Supplementary data

Supplementary data to this article can be found online at https://doi.org/10.1016/j.msec.2019.110209.

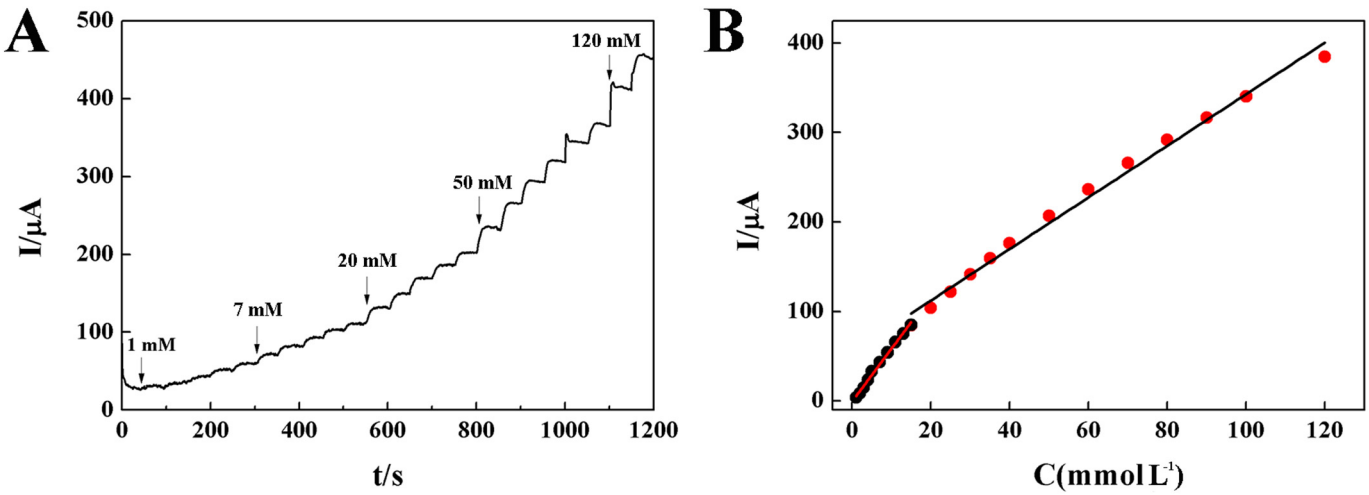

Fig. 5. (A) Amperometric response of Nafion/Hb/Co_3O_4–CNF/CILE at −0.55 V for the sequential additions of varying concentrations of TCA into a continuously stirred pH 5.0 PBS; (B) The linear relationship between I_{ss} and TCA concentration.

Table 3
Electrochemical detection of real samples (n = 3).

Sample	Marked (mmol L^{-1})	Detected (mmol L^{-1})	Added (mmol L^{-1})	Total (mmol L^{-1})	Recovery (%)	RSD (%)
35% Medical facial peel solution	27.17	27.15	10.00	37.33	101.80	1.26
			20.00	47.18	99.90	0.86
			30.00	57.12	99.90	0.39
			40.00	67.12	99.92	0.31
Soak water of pickled vegetables	unknown	2.61	1.00	3.59	98.00	0.28
			2.00	4.63	101.00	1.09
			3.00	5.64	101.00	1.95

References

[1] P. Das, M. Das, S.R. Chinnadayyala, I.M. Singha, P. Goswami, Recent advances on developing 3rd generation enzyme electrode for biosensor applications, Biosens. Bioelectron. 79 (2016) 386–397.
[2] A.D. Hirst, J.F. Stevens, Electrodes in clinical chemistry, Ann. Clin. Biochem. 22 (1985) 460–488.
[3] W. Sun, S.X. Gong, F. Shi, L.L. Cao, L.Y. Ling, W.Z. Zheng, W.C. Wang, Direct electrochemistry and electrocatalysis of hemoglobin in graphene oxide and ionic liquid composite film, Mater. Sci. Eng. C 40 (2014) 235–241.
[4] S. Alim, A.K.M. Kafi, R. Jose, M.M. Yusoff, J. Vejayan, Enhanced direct electron transfer of redox protein based on multiporous SnO_2, nanofiber-carbon nanotube nanocomposite and its application in biosensing, Int. J. Biol. Macromol. 114 (2018) 1071–1076.
[5] B. Willner, E. Katz, I. Willner, Electrical contacting of redox proteins by nanotechnological means, Curr. Opin. Biotechnol. 17 (2006) 589–596.
[6] R.A. Marcus, N. Sutin, Electron transfers in chemistry and biology, Biochim. Biophys. Acta 811 (1985) 265–322.
[7] M. Baghayeri, E.N. Zare, R. Hasanzadeh, Facile synthesis of PSMA-g-3ABA/MWCNTs nanocomposite as a substrate for hemoglobin immobilization: application to catalysis of H_2O_2, Mater. Sci. Eng. C 39 (2014) 213–220.
[8] M. Baghayeri, H. Veisi, Fabrication of a facile electrochemical biosensor for hydrogen peroxide using efficient catalysis of hemoglobin on the porous Pd@Fe_3O_4-MWCNT nanocomposite, Biosens. Bioelectron. 74 (2015) 190–198.
[9] M. Baghayeri, E.N. Zare, M.M. Lakouraj, Novel superparamagnetic PFu@Fe_3O_4 conductive nanocomposite as a suitable host for hemoglobin immobilization, Sens. Actuators, B 202 (2014) 1200–1208.
[10] M. Baghayeri, E.N. Zare, M.M. Lakouraj, A simple hydrogen peroxide biosensor based on a novel electro-magnetic poly(p-phenylenediamine)@Fe_3O_4 nanocomposite, Biosens. Bioelectron. 55 (2014) 259–265.
[11] S. Palanisamy, S. Cheemalapati, S.M. Chen, Highly sensitive and selective hydrogen peroxide biosensor based on hemoglobin immobilized at multiwalled carbon nanotubes-zinc oxide composite electrode, Anal. Biochem. 429 (2012) 108–115.
[12] V. Velusamy, S. Palanisamy, S.M. Chen, T.W. Chen, S. Selvam, S.K. Ramaraj, B.S. Lou, Graphene dispersed cellulose microfibers composite for efficient immobilization of hemoglobin and selective biosensor for detection of hydrogen peroxide, Sens. Actuators, B 252 (2017) 175–182.
[13] B. Thirumalraj, S. Palanisamy, S.M. Chen, K.D. Wael, A graphene/gelatin composite material for the entrapment of hemoglobin for bioelectrochemical sensing applications, J. Electrochem. Soc. 163 (2016) B265–B271.
[14] S. Palanisamy, Y.T. Wang, S.M. Chen, B. Thirumalraj, B.S. Lou, Direct electrochemistry of immobilized hemoglobin and sensing of bromate at a glassy carbon electrode modified with graphene and β-cyclodextrin, Microchim. Acta 183 (2016) 1953–1961.
[15] S. Palanisamy, C. Karuppiah, S.M. Chen, P. Periakaruppan, A highly sensitive and selective enzymatic biosensor based on direct electrochemistry of hemoglobin at zinc oxide nanoparticles modified activated screen printed carbon electrode, Electroanalysis 26 (2014) 1984–1993.
[16] S. Palanisamy, V. Velusamy, S.W. Chen, T.C.K. Yang, S. Balu, C.E. Banks, Enhanced reversible redox activity of hemin on cellulose microfiber integrated reduced graphene oxide for H_2O_2 biosensor applications, Carbohydr. Polym. 204 (2019) 152–160.
[17] S. Radhakrishnan, S.J. Kim, An enzymatic biosensor for hydrogen peroxide based on one-pot preparation of CeO_2-reduced graphene oxide nanocomposite, RSC Adv. 5 (2015) 12937–12943.
[18] S. Radhakrishnan, K. Krishnamoorthy, C. Sekar, J. Wilson, S.J. Kim, A highly sensitive electrochemical sensor for nitrite detection based on Fe_2O_3 nanoparticles decorated reduced graphene oxide nanosheets, Appl. Catal., B 148 (2014) 22–28.
[19] C. Zhu, G. Yang, H. Li, D. Du, Y.H. Lin, Electrochemical sensors and biosensors based on nanomaterials and nanostructures, Anal. Chem. 87 (2018) 230–249.
[20] S. Ranjbar, S. Shahrokhian, Design and fabrication of an electrochemical aptasensor using Au nanoparticles/carbon nanoparticles/cellulose nanofibers nanocomposite for rapid and sensitive detection of Staphylococcus aureus, Bioelectrochemistry 123 (2018) 70–76.
[21] J.N. Tiwari, V. Vij, K.C. Kemp, Engineered Carbon-nanomaterial based electrochemical sensors for biomolecules, ACS Nano 10 (2015) 46–80.
[22] E. Sapountzi, M. Braiek, J.F. Chateaux, J.R. Nicole, L. Florence, Recent advances in electrospun nanofiber interfaces for biosensing devices, Sensors 17 (2017) 1887–1914.
[23] A. Walcarius, S.D. Minteer, J. Wang, Y.H. Lin, A. Merkoçi, Nanomaterials for biofunctionalized electrodes: recent trends, J. Mater. Chem. B. 1 (2013) 4878–4908.
[24] Y. Zhang, Q. Wei, The role of nanomaterials in electroanalytical biosensors: a mini review, J. Electroanal. Chem. 781 (2016) 401–409.
[25] M. Holzinger, A.L. Goff, S. Cosnier, Nanomaterials for biosensing applications: a review, Front. Chem. 2 (2014) 63–72.
[26] J. Kim, R. Kumar, A.J. Bandodkar, J. Wang, Advanced materials for printed wearable electrochemical fevices: a review, Adv. Electron. Mater. 3 (2017) 1600260–1600274.
[27] A. Othman, A. Karimi, S. Andreescu, Functional nanostructures for enzyme based biosensors: properties, fabrication and applications, J. Mater. Chem. B. 4 (2016) 7178–7203.
[28] S. Babitha, L. Rachita, K. Karthikeyan, E. Shoba, I. Janani, B. Poornima, K.P. Sai, Electrospun protein nanofibers in healthcare: a review, Int. J. Pharm. 523 (2017) 52–90.
[29] X. Zhang, D. Liu, B. Yu, T.Y. You, A novel nonenzymatic hydrogen peroxide sensor

based on electrospun nitrogen-doped carbon nanoparticles-embedded carbon nanofibers film, Sens. Actuators, B 224 (2016) 103–109.
[30] Q.H. Guo, L.J. Liu, T.T. Wu, Q.Q. Wang, H.H. Wang, J.Y. Liang, S.L. Chen, Flexible and conductive titanium carbide-carbon nanofibers for high-performance glucose biosensing, Electrochim. Acta 281 (2018) 517–524.
[31] K. Mondal, M.A. Ali, C. Singh, G. Sumana, B. Malhotra, A.S. IITK, Highly sensitive porous carbon and metal/carbon conducting nanofiber based enzymatic biosensors for triglyceride detection, Sens. Actuators, B 246 (2017) 202–214.
[32] Y.C. Zhu, Y.T. Xu, Y. Xue, G.C. Fan, P.K. Zhang, W.W. Zhao, J.J. Xu, H.Y. Chen, Three-dimensional CdS@carbon fiber networks: innovative synthesis and application as a general platform for photoelectrochemical bioanalysis, Anal. Chem. 91 (2019) 6419–6423.
[33] W. Chen, W.J. Weng, C.X. Yin, X.L. Niu, G.J. Li, H. Xie, J. Liu, W. Sun, Fabrication of an electrochemical biosensor based on Nafion/Horseradish Peroxidase/Co_3O_4 NP/CILE and its electrocatalysis, Int. J. Electrochem. Sci. 13 (2018) 4741–4752.
[34] H.K. Lei, W. Sun, Z.F. Sun, Amorphous Co_3O_4-decorated Pd as an efficient electrocatalyst for methanol oxidation, Nano 12 (2017) 1750078–1750085.
[35] B.G. Mohammad, S. Mohammad, Sensitive warfarin sensor based on cobalt oxide nanoparticles electrodeposited at multi-walled carbon nanotubes modified glassy carbon electrode (Co_xO_yNPs/MWCNTs/GCE), Electrochim. Acta 246 (2017) 689–698.
[36] V. Usai, T. Mugadza, F. Chigondo, Synthesis and characterisation of cobalt oxide nanoparticles decorated graphene oxide and its electrocatalytic behavior, Polyhedron (157) (2019) 192–199.
[37] Y. Li, F.M. Li, X.Y. Meng, S.N. Li, J.H. Zeng, Y. Chen, Ultrathin Co_3O_4 nanomeshes for the oxygen evolution reaction, ACS Catal. 8 (2018) 1913–1923.
[38] Y. Li, F.M. Li, X.Y. Meng, X.R. Wu, S.N. Li, Y. Chen, Direct chemical synthesis of ultrathin holey iron doped cobalt oxide nanosheets on nickel foam for oxygen evolution reaction, Nano Energy 54 (2018) 238–250.
[39] S.Z. Zhao, B. Guo, G.Y. Han, Y.N. Tian, Metallization of electrospun polyacrylonitrile fibers by gold, Mater. Lett. 62 (2008) 3751–3753.
[40] H.Y. Liu, L. Xu, X.P. Tang, S.I. Na, Fabrication of aligned PAN nanofiber by electrospinning with parallel electrode, Adv. Mater. Res. 905 (2014) 19–22.
[41] W. Sun, Y.Z. Li, Y.Y. Duan, K. Jiao, Direct electrocatalytic oxidation of adenine and guanine on carbon ionic liquid electrode and the simultaneous determination, Biosens. Bioelectron. 24 (2009) 988–993.
[42] X.L. Niu, X.Y. Li, W. Chen, X.B. Li, W.J. Weng, C.X. Yin, R.X. Dong, W. Sun, G.J. Li, Three-dimensional reduced graphene oxide aerogel modified electrode for the sensitive quercetin sensing and its application, Mater. Sci. Eng. C 89 (2018) 230–236.
[43] T.T. Yang, M.L. Du, H. Zhu, M. Zhang, M.L. Zou, Immobilization of Pt nanoparticles in carbon nanofibers: bifunctional catalyst for hydrogen evolution and electrochemical sensor, Electrochim. Acta 167 (2015) 48–54.
[44] K.B. Oldham, Analytical expressions for the reversible Randles-Sevcik function, J. Electroanal. Chem. 105 (1979) 373–375.
[45] A.E.F. Nassar, Z. Zhang, N.F. Hu, J.F. Rusling, Proton-coupled electron transfer from electrodes to myoglobin in ordered biomembrane-like films, J. Phys. Chem. B 101 (1997) 2224–2231.
[46] A.J. Bard, L.R. Faulkner, Electrochemical Methods: Fundamentals and Application, Wiley, New York, 1980, pp. 459–462.
[47] S.F. Wang, T. Chen, Z.L. Zhang, X.C. Shen, Z.X. Lu, D.W. Pang, K.Y. Wong, Direct electrochemistry and electrocatalysis of heme proteins entrapped in agarose hydrogel films in room-temperature ionic liquids, Langmuir 21 (2005) 9260–9266.
[48] E. Laviron, General expression of the linear potential sweep voltammogram in the case of diffusion less electrochemical systems, J. Electroanal. Chem. 101 (1979) 19–28.
[49] X.Y. Li, X.L. Niu, W.S. Zhao, W. Chen, C.X. Yin, Y.L. Men, G.J. Li, W. Sun, Black phosphorene and PEDOT:PSS-modified electrode for electrochemistry of hemoglobin, Electrochem. Commun. 86 (2018) 68–71.
[50] Y.Y. Niu, R.Y. Zou, H.A. Yones, X.B. Li, X.Y. Li, X.L. Niu, Y. Chen, P. Li, W. Sun, Electrochemical behavior of horseradish peroxidase on WS_2 nanosheet-modified electrode and electrocatalytic investigation, J. Chin. Chem. Soc. 65 (2018) 1127–1135.
[51] F. Valentini, L. Cristofanelli, M. Carbone, G. Palleschi, Glassy carbon electrodes modified with hemin-carbon nanomaterial films for amperometric H_2O_2 and NO_2^- detection, Electrochim. Acta 63 (2012) 37–46.
[52] Z.H. Zhu, L.N. Qu, X. Li, Y. Zeng, W. Sun, X.T. Huang, Direct electrochemistry and electrocatalysis of hemoglobin with carbon nanotube-ionic liquid-chitosan composite materials modified carbon ionic liquid electrode, Electrochim. Acta 55 (2010) 5959–5965.
[53] T.R. Zhan, M.Y. Xi, Y. Wang, W. Sun, W.G. Hou, Direct electrochemistry and electrocatalysis of myoglobin immobilized on Fe_2O_3 nanoparticle-sodium alginate-ionic liquid composite-modified electrode, J. Colloid Interface Sci. 346 (2010) 188–193.
[54] G.L. Turdean, G. Szabo, Nitrite detection in meat products samples by square-wave voltammetry at a new single walled carbon naonotubes-myoglobin modified electrode, Food Chem. 179 (2015) 325–330.
[55] J.J. Yu, J.R. Ma, F.Q. Zhao, B.Z. Zeng, Direct electron-transfer and electrochemical catalysis of hemoglobin immobilized on mesoporous Al_2O_3, Electrochim. Acta 53 (2008) 1995–2001.